Journal of Alloys and Compounds 809 (2019) 151780

Contents lists available at ScienceDirect

Journal of Alloys and Compounds

journal homepage: http://www.elsevier.com/locate/jalcom

Assessing microstructure and mechanical behavior changes in a Sn-Sb solder alloy induced by cooling rate

Aline Ferreira Schon [a], Rodrigo Valenzuela Reyes [b], José Eduardo Spinelli [b, c, *], Amauri Garcia [d], Bismarck Luiz Silva [a]

[a] Department of Materials Engineering, Federal University of Rio Grande do Norte-UFRN, 59078-970, Natal, Brazil
[b] Federal University of São Carlos, Graduate Program in Materials Science and Engineering, 13565-905, São Carlos, SP, Brazil
[c] Department of Materials Engineering, Federal University of São Carlos, UFSCar, 13565-905, São Carlos, SP, Brazil
[d] Department of Manufacturing and Materials Engineering, University of Campinas UNICAMP, 13083-860, Campinas, SP, Brazil

ARTICLE INFO

Article history:
Received 17 May 2019
Received in revised form
7 August 2019
Accepted 8 August 2019
Available online 9 August 2019

Keywords:
Sn-Sb alloy
Solders
Solidification
Microstructure
Tensile behavior

ABSTRACT

In the present investigation a directional solidification experiment was performed in order to examine distinct microstructures related to different slices of the solidified Sn-2 wt.%Sb alloy casting. Such alloy is an alternative of interest with the target of replacing lead-containing solder alloys (containing 85 to 97 wt% of Pb) given that lead (Pb) is considered an important environmental complaint and has devastating effects on the human body. The imposed conditions in the present experiment may lead to solutal and thermal stability of the melt throughout solid growth towards the liquid. It was found that Sn-rich cells may prevail for cooling rates higher than 1.0 K/s whereas only Sn-rich dendrites appear for specimens solidified at rates lower than 0.3 K/s. The growth of dendrites is delayed when compared to previous results in the literature. In the presence of convective flow originated either thermally or solutally, β-Sn dendrites were reported to grow for samples solidified at rates as high as 1.5 K/s (i.e., 5 times higher). It appears that convection currents induce instabilities to happen at the solidification front and the growth of dendrites is benefited over such conditions. Tensile tests were also performed for Sn-Sb samples having distinct cellular and dendritic dimensions. It was found that unstable plastic flow happened during all tensile tests. The formation of bands along a specimen gauge was recognized as being a manifestation of the Portevin – Le Chatelier (PLC) effect. A homogeneous deformation stage preceded the start of serrations of stresses in the samples of the investigated alloy. The amplitudes of the serrations were found to be lower in the samples having cells as compared to those associated with dendritic microstructures.

1. Introduction

Throughout the past few decades Pb-based and eutectic Pb-Sn alloys have become extensively used in soldering processes. However, considering that Pb is a toxic metal, its use has been lowered through the claim of environmental directives such as the Restriction of Hazardous Substances (RoHS), as proposed by the European Union [1], being firstly applied in 2011. For instance, from the industrial viewpoint the concession for the use of Pb is allowed for automotive parts until 2023 [2,3].

In addition to environmental problems, some soldering methods may employ alloys characterized by the occurrence of transformations other than the eutectic one. These alloys may have higher melting temperatures as well as the aggregation of more complex transformations, such as the peritectic one. Although the peritectic alloys represent an important class of industrial materials [4–6], Sn-Cu and Sn-Sb alloys [7,8] are the single tin-based alloys available to be employed in soldering as lead-free materials. Peritectic transformations characterize such alloys during cooling from the liquid.

Monophasic Sn-Sb Pb-free solder alloys arouse interest due to possibility of application as high temperature material in step soldering practices. Various advantages are related to the said alloys: better strength as compared to Pb-Sn alloys, better room temperature creep resistance and ductility, and higher microstructure

* Corresponding author. Federal University of São Carlos, Graduate Program in Materials Science and Engineering, 13565-905, São Carlos, SP, Brazil.
E-mail address: spinelli@ufscar.br (J.E. Spinelli).

https://doi.org/10.1016/j.jallcom.2019.151780
0925-8388/

stability [9–14]. It is worth noting that transient solidification conditions characterize the soldering processes during the cooling of the solder joint. Emphasizing this characteristic, the heat flow regime becomes of prime importance since it is known that the transient growth of solidification microstructures is less understood during peritectic transformation. This is the case, for example, of Sn-Sb alloys, for which the literature, to the best of the authors' knowledge, endures scarce in terms of characterization of microstructures and determination of properties. Growth laws for industrial scenarios in peritectic transformations are yet quite untouched on the level of scaling laws. However, such laws are essential for a general understanding of the microstructural evolution, which can be very useful for pre-programming purposes dedicated to the soldering operations.

The peritectic reaction occurring during cooling of the tin-rich Sn-Sb solder alloys is: L + Sn_3Sb_2 (α) > Sn (β), at 243 °C [15]. It is important to emphasize that the selection of microstructures in peritectic systems is mostly governed by concurrent effects like convection, morphology of the resulting β phase and cooling rate. Kim et al. [16] demonstrated that the resulting microstructure of the near-peritectic Sn-5 wt.%Sb alloy solidified in air is constituted by both β-Sn and α-SbSn phases.

Although previous studies have been devoted to the characterization of the Sn-2 wt.%Sb alloy in terms of microstructure, that is, either dendritic or cellular arrangements [8,17], the visualization of dendrites when the solidification process is carried out vertically upwards has not been realized. It is well known that the effect of the solidification growth direction in the formed microstructure and morphology may be considerably important for processes where the solid may grow following different orientations with respect to the gravity, that is, for conditions with the surface causing cooling placed on the bottom, the top or the side of the solidified volume.

Dias et al. [8] examined Sn-2 wt.%Sb alloy samples solidified at rates ranging from 1.0 K/s to 40 K/s. These samples were a result of a casting directionally solidified (DS) vertically upwards in a water-cooled mold. Despite suppressing convection action, a single growth of high-cooling rate cells was obtained in this case. Another investigation [17], in turn, demonstrated the growth of fully cellular portions for cooling rates higher than 5.0 K/s as well as fully dendritic array for cooling rates lower than 1.5 K/s. Despite characterizing a cellular/dendritic reverse transition in the Sn-2 wt.%Sb alloy, the solidification occurred horizontally, which causes convection, thanks to the solutal gradients existing in the liquid. As such, the observed dendritic array is a result of dendrite tips growing against a moving liquid ahead the solidification front.

The aforementioned investigations [8,17] also demonstrated that the tensile strength of the Sn-2 wt.%Sb alloy for samples having the Sn (β) matrix with a cellular morphology, remained unaffected even with the variations in the cell size. Considering the samples associated with the dendritic microstructural zone, slight decrease in the tensile strength with increasing length scale of the dendritic microstructure is reported. In addition to considering mechanical properties like strength and ductility, other effects associated with plastic instabilities during loading may require attention. One of these effects is the Portevin - Le Chatelier (PLC) [18]. Its occurrence is more frequently associated with industrial materials such as steel and aluminum alloys, being much less investigated for Sn-based solders. The localized deformation associated with the PLC effect causes structural problems. The most reported consequence of such instabilities in industrial parts is the development of rough and unsightly markings on the surfaces during shape-forming processes [19]. Some other negative qualities can be related to PLC, that is, decrease in ductility, reduction in fracture toughness and increase in work hardening rate [19].

The PLC manifestation is referred to serrated flow in the plastic regime of the stress-strain plots. Previous investigations about localized deformation bands in specimens of Al and Mg based alloys demonstrated that the repetitive yielding is a consequence of dynamic interactions between mobile dislocations and diffusing solute atoms clustered around these dislocations during plastic regime. The solutes continually block and release the mobile dislocations [18,20]. Stress discontinuity is often observed when a specimen of a dilute alloy is strained in uniaxial loading [20]. Another point that deserves attention is the extension (variations of tensile stress) of these serrations, considering different growth morphologies, such as dendritic and cellular.

Quantification of the bands and their motions and their relations with features of the microstructure still remains challenging. Cai et al. [21] demonstrated that Mg chemistry in Al-Mg alloys plays a fundamental role on the serration characteristics (the serration type and amplitude). Further, Mg content may shift the region in which the PLC effect occurs to high strain rate. Generically three types of serrations and the associated bands are founded [20]: type A - continuously propagating and associated with small stress drops; type B - each new single band starts above the one preceding; and type C - randomly nucleated static bands with large and regular distributed stress drops.

Even though previous investigations on Sn-Sb alloys existing in the literature emphasize the growth of cells and dendrites, the growth of dendrites with absence of convection in the melt still deserves attention. Furthermore, correlations of mechanical properties with dimensional parameters of the dendritic microstructure are still unknown, considering solidification conditions comparable to those found in soldering processes. In the present work, the evolution of the solidification cooling rate during upward directional solidification of the Sn-2 wt.%Sb alloy will be determined and the phases composing the microstructure will be subjected to a comprehensive characterization by X-ray diffraction (XRD), Optical Microscopy and Scanning Electron Microscopy (SEM). The performed characterization methods will allow the selection of regions of predominance of either cells or dendrites as well as their related ranges of cooling rates. A comparative analysis of the present results with those demonstrated by using distinct solidification setups and higher cooling rates will be undertaken. Additionally, another attention is particularly focused on the variation of the stress serration amplitude due to the PLC effect with the form of the Sn-rich phase, i.e., cellular or dendritic.

2. Experimental procedure

Monophasic Sn-2 wt.%Sb alloys castings were produced using commercially pure Sn (99.96%) and Sb (99.63%), which were melted inside a SiC crucible in a muffle furnace, homogenized and poured into a stainless-steel split mold. This type of mold allows a change in the surface of a 3 mm-thick steel bottom part (closure mold device) by applying coatings of insulating materials. In the case of the present experiments, a 100 μm-thick layer of silica-alumina ceramic was coated on the active surface of the bottom part so that a decrease in the cooling rates during the solidification progress across the DS casting is achievable. This adaptation was necessary since high cooling rate cells were already demonstrated for cooling rates exceeding 1 K/s in a previous investigation with the same alloy of interest [8]. The goal at this point was to obtain both cellular and dendritic microstructural zones in a single DS casting. Painting the active surface of the bottom part could permit cooling rates lower than 1 K/s to be attained in the very first portions of the casting with respect to the cooled surface.

After natural solidification within the mold, the alloy was remelted *in situ* by radial electrical wiring positioned around a

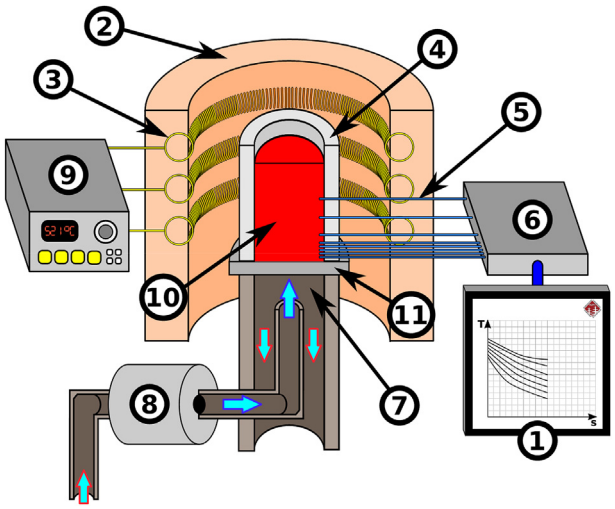

Fig. 1. Scheme of the upward directional solidification system used to generate the Sn-Sb alloy casting: 1 - acquired thermal profiles during experiment; 2 - ceramic support; 3 - electric resistances; 4 - stainless-steel split mold; 5 - thermocouples; 6 - data logger; 7 - water flow inlet; 8 - flowmeter; 9 - temperature controller; 10 - molten alloy and 11 - cooled bottom part.

stainless-steel split mold, as can be seen in the solidification apparatus scheme in Fig. 1. Then, when the melt temperature is about 10% above the liquidus temperature, the electric heaters are disconnected and at the same time the water flow at the bottom of the container is started, which allows the onset of directional solidification. The evolution of temperatures along the length of the casting was monitored by fine type J thermocouples (0.2 mm diameter wire), placed in the geometrical center of the cylindrical mold cavity, but in various relative positions along its length. The determination of the tip cooling rate, $\dot{T}_L$, as a function of position (P) in the casting was carried out by computing the time-derivative of each cooling curve (dT/dt) right after the passage of the liquidus isotherm by each thermocouple.

The dimensions of the stainless steel mold were: internal diameter of 60 mm, height of 157 mm and wall thickness of 5 mm. The lateral inner mold surface was covered with a 2 mm-thick layer of insulating mass of silica-alumina ceramic to minimize radial heat losses and assist the removal of the castings. Additional information on specific details of the directional solidification procedure can be found in previous studies [22–24].

The considerations about microstructure were focused on two steps: firstly, micrographs were assessed and extensively examined by using an optical microscope so that zones containing Sn-rich phase in the form of cells, cells + dendrites and dendrites could be classified according to the distinct slices removed from the DS casting; and secondly, measuring the dimensions of the cells and dendrites with basis on the well-known methods to determine cellular spacing and primary dendrite arm spacing. These are the best measurable parameters to represent the effects of solidification conditions on the as-solidified microstructure. For this purpose, selected transverse (perpendicular to the growth direction) and longitudinal samples were extracted at different positions along the length of the DS casting for metallography.

The cellular spacing (λc) and primary dendrite arm spacing (λ_1) were measured from the optical images of the samples: about 30 measurements at each selected section. The same samples were used for the X-ray diffraction (XRD) analysis. A Shimadzu diffractometer (Kyoto, Japan) was employed to obtain the XRD patterns under the 2θ range from 25° to 80° using Cu Kα radiation with a wavelength of 0.15406 nm. A Scanning Electron Microscope (SEM) from Zeiss (Oberkochen, Germany, Auriga 40 model) was used in order to characterize the stage of formation of the β phase for samples solidified at distinct cooling rates.

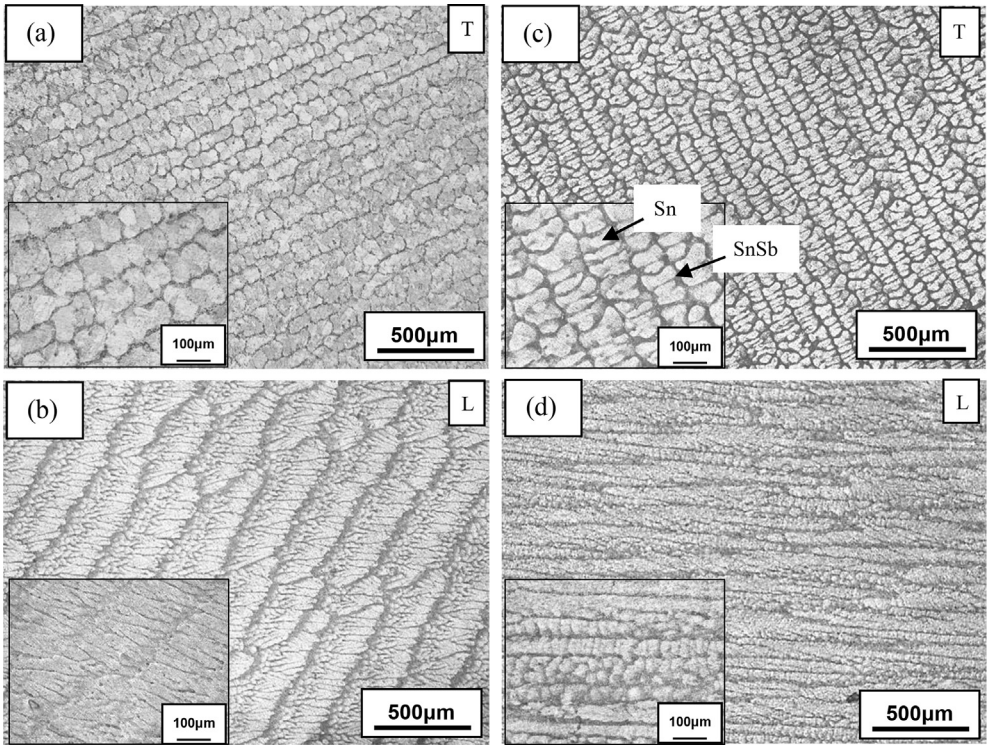

Fig. 2. Growth of β-Sn cells in the first segments of the directionally solidified Sn-Sb casting. The optical images are related to the achieved thermal parameters: (a,b) $\dot{T} = 2.7$ K/s; $V_L = 0.31$ mm/s and (c,d) $\dot{T} = 1.1$ K/s; $V_L = 0.27$ mm/s. T: transverse and L: longitudinal specimens with respect to the vertical axis of growth.

Transverse specimens were extracted from different positions along the length of the DS casting, and prepared for tensile testing according to specifications of ASTM Standard E 8 M. A strain rate of about $3 \times 10^{-3}\,s^{-1}$ was adopted. In order to ensure the reproducibility of results, four specimens were tested for each selected position, and tensile properties were determined: ultimate tensile strength (σ_u) and elongation (δ). PLC effects were observed in all plotted stress-strain diagrams. Therefore, the PLC band propagative characteristics were examined for all microstructure configurations with basis on the serration types, stress amplitudes and strains

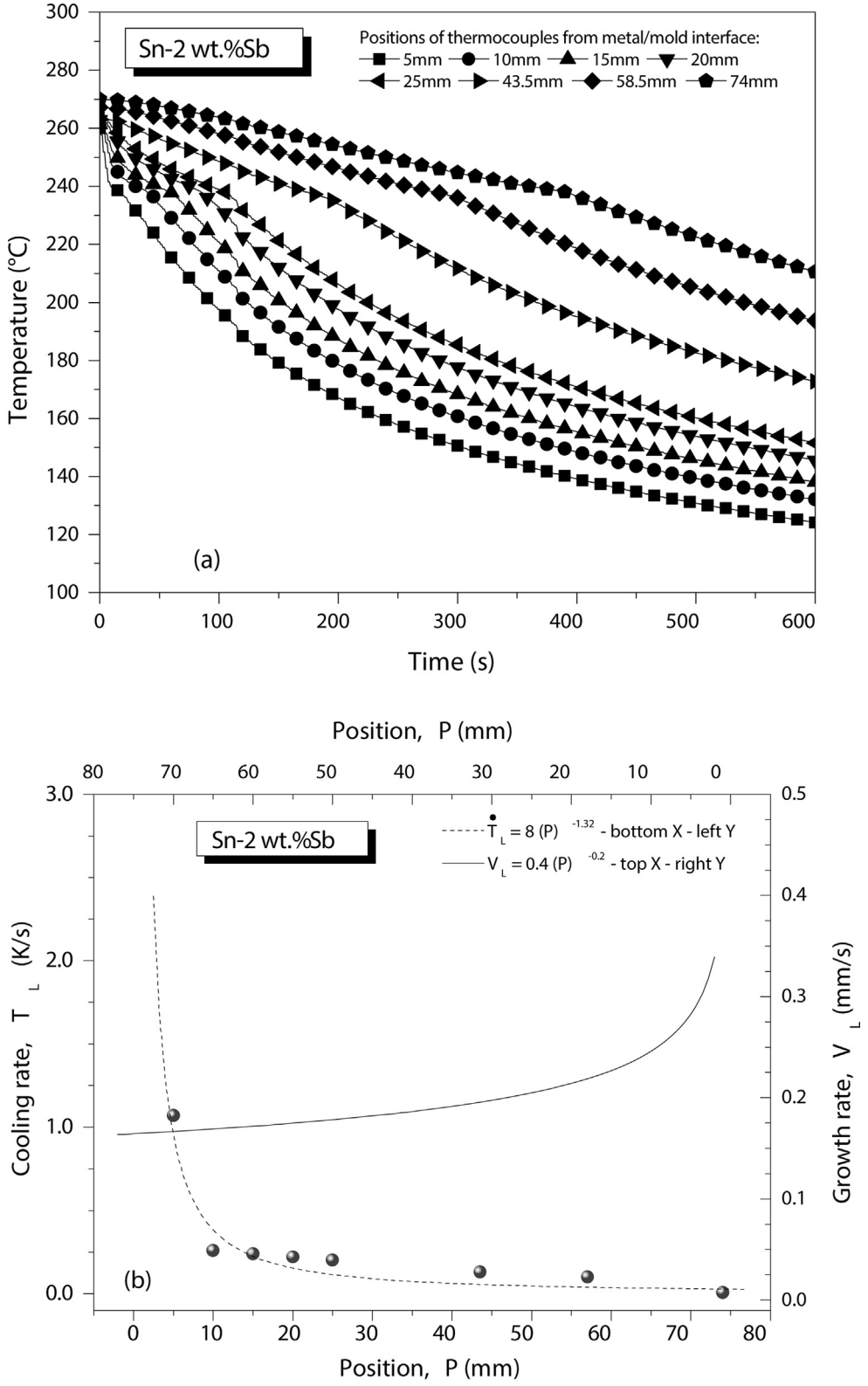

Fig. 3. (a) Cooling curves at different positions within the DS casting; (b) cooling rate and growth rate as a function of position in the Sn-Sb alloy casting.

associated with the beginning of the jerky flow.

3. Results and discussions

Characteristic transverse and longitudinal optical microstructures can be seen in Fig. 2. It refers to the current β-Sn phase morphologies in the first microstructural zone placed near the water-cooled surface of the Sn-2 wt.%Sb alloy casting. The presence of cells can be noted for the related cooling rates of 2.7 K/s and 1.1 K/s. These values were obtained from the experimental plots given in Fig. 3. The microstructures are constituted by a Sn-rich matrix (β-Sn phase) surrounded by the Sn-Sb (α) phase (darker regions in Fig. 2). The zone corresponding to relatively high cooling rates and growth rates develops very fine interface structures during the growth process. It appears that under such settings the dendritic tips become so fine that cellular structures develop. At a position about 5 mm from the cooled surface (i.e., $\dot{T}_L = 1.1$ K/s), the microstructure begins to reveal onset of dendritic features, characterized by initial perturbations on the cellular pattern. However, the effective growth of lateral branches is more remarkable for positions associated with cooling rates ranging from 0.3 K/s to 1.0 K/s, but occurring in concurrence with cells. Such microstructural zone was defined either as transition zone or as cell + dendrite zone.

A previous study performed with a Sn-0.2 wt%Ni alloy solidified vertically upwards in a steel cooled mold demonstrated a critical value of 1.2 K/s for the prevalence of high cooling rate cells [25], which is quite similar to the results found in the present investigation. Both studies resulted in the melt being solutally and thermally stable since the rejection of either Sb or Ni at the solidification front induces the local incidence of solute-enriched liquids denser than the open liquid. The bottom-to-top growth configuration also results in the temperature increasing from the solidification front to the top. Hence, convection is inhibited in both cases.

Results found for unstable conditions of solidification with regard to the melt convection, in contrast, stressed that cells may happen for higher cooling rates. For example, one investigation with the Sn-0.2 wt%Ni alloy subjected to the bottom-to-top growth in a copper cooled mold demonstrated the growth of cells for $\dot{T} >$ 5.5 K/s [26]. Another investigation [17] categorized a region of completely cellular microstructure happening thanks to $\dot{T}$ higher than 5.0 K/s throughout the horizontal growth of the Sn-2 wt.%Sb alloy. In both cases, the growth of cells is related to high cooling rates due to the strong instabilities on the solid/liquid interface for slower cooling conditions. In the case of the Sn-Ni alloy, the instabilities are motivated by the dissolution of copper from the mold into the liquid [27]. In the case of the study with the Sn-2 wt.%Sb alloy [17], the growth direction configuration induces thermal and solutal convection at the growth front, which prevents the cellular morphology to occur for slower cooling conditions.

For regions farther from the cooled surface of the casting (i.e., P > 20 mm), the matrix starts to develop a dendritic microstructure as shown in Fig. 4, right after the transition zone in the casting. This characterizes an unexpected reverse dendritic/cellular transition. The micrographs in Fig. 4 show secondary arms branching out from the primary arms, which characterize very clearly the development of a dendritic array. The dendritic microstructure zone occurred for $\dot{T} < 0.3$ K/s. The growth of dendrites is delayed as compared to previous results [17] with the same alloy solidified horizontally. In this case, the critical cooling rate for obtaining dendritic morphology is lower than 1.5 K/s.

In order to prove the experimental variation of the microstructural spacing with the cooling rate, a plot of the related quantities is given in Fig. 5. The quantities associated with the transition zone are preferred to be omitted since no prevalent morphology happens.

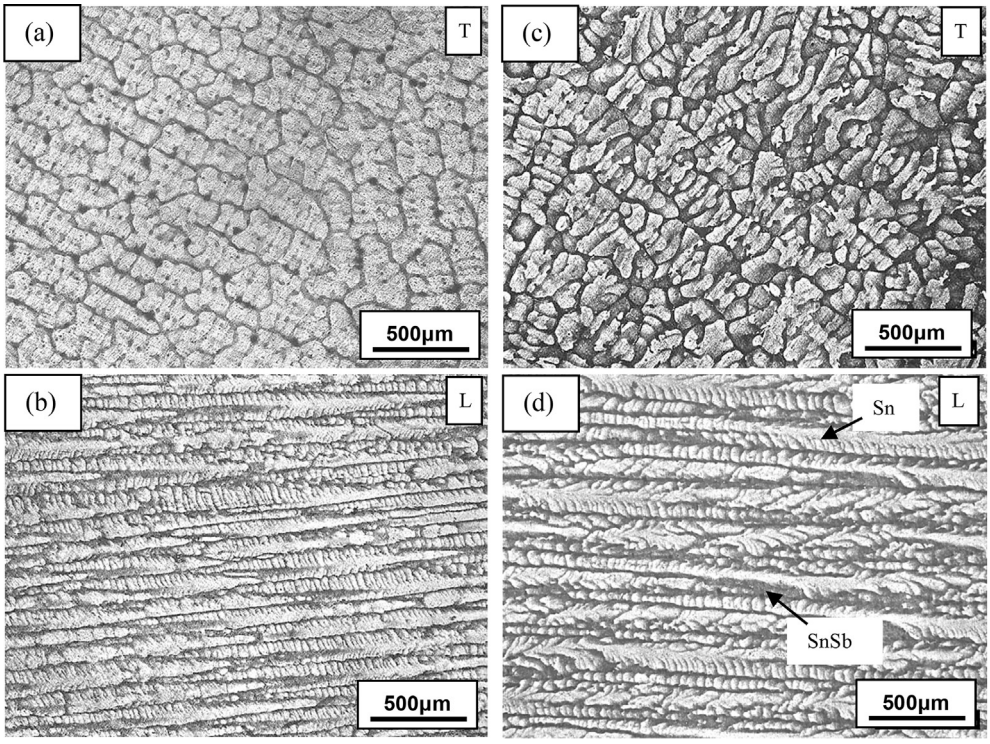

Fig. 4. Growth of β-Sn phase in the form of dendrites for positions farther from the bottom of the directionally solidified Sn-Sb casting. The optical images are related to the achieved thermal parameters: (a,b) $\dot{T} = 0.25$ K/s; $V_L = 0.22$ mm/s and (c,d) $\dot{T} = 0.07$ K/s; $V_L = 0.16$ mm/s. T: transverse and L: longitudinal specimens with respect to the vertical axis of growth.

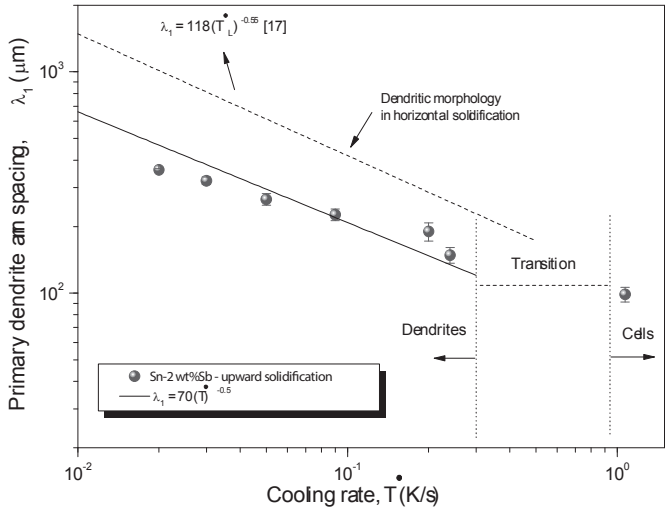

Fig. 5. Variation of the primary dendritic spacing with cooling rate plotted for the Sn-2 wt.%Sb alloy.

Little research has been devoted on the effect of melt convection on the primary dendritic/cellular spacing in peritectic alloys. In the case of the Sn-2 wt.%Sb alloy, the possibility is to compare very different solidification conditions between each other, which are that executed here (i.e., very weak convection) and that performed by Rocha et al. [17] (strong melt convection). The power function relationships $\lambda_1 = 70\ (\dot{T})^{-0.5}$ and $\lambda_1 = 118\ (\dot{T})^{-0.55}$ represent the dendritic growth for the samples solidified at weak and strong melt convection respectively. The exponents are quite similar. However, the multipliers differ in 70%. Convection gives rise to the enhancement of the solute diffusion, reducing the solute boundary layer [28]. Under such conditions, the formed thin peritectic β layers are preferentially dissolved due to the strong convection currents. As a consequence, the lateral growth of the α phase (SnSb) is benefited, which promotes a resulting increase in λ_1. Fig. 6 shows schematically the dissolution of dendrites in the samples with strong melt convection. Further, the dissolution of the β phase into the liquid constrains the mechanism of nucleation from this phase

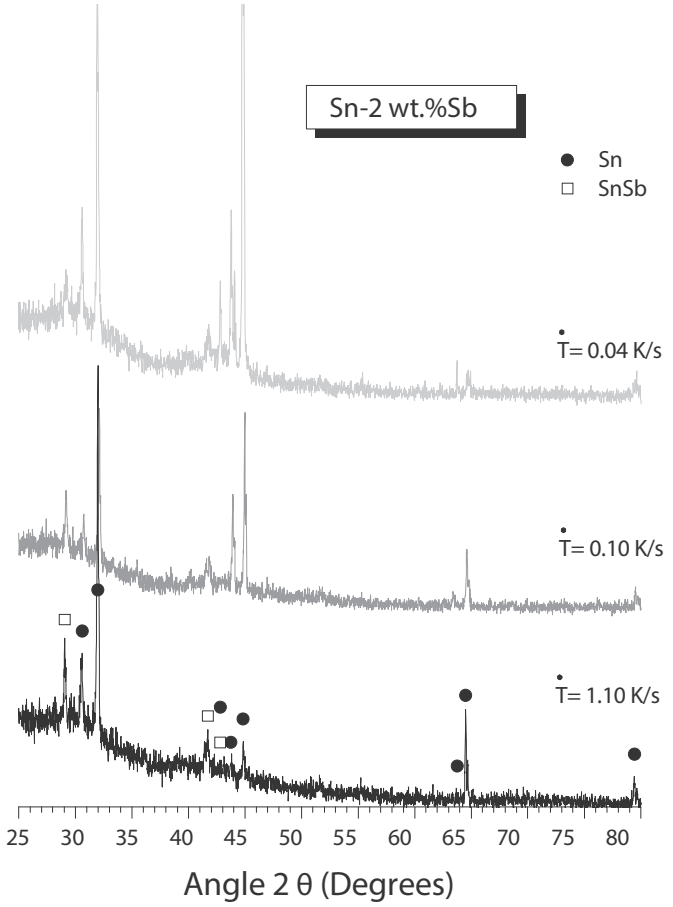

Fig. 7. X-ray diffraction (XRD) patterns for Sn-2 wt.%Sb samples solidified at three distinct solidification cooling rates.

of fresh primary dendritic stems, lowering the local volume fraction of dendrites.

Both α (SnSb) and β (Sn) phases constituting the microstructures found in the present investigation are confirmed by XRD analyses

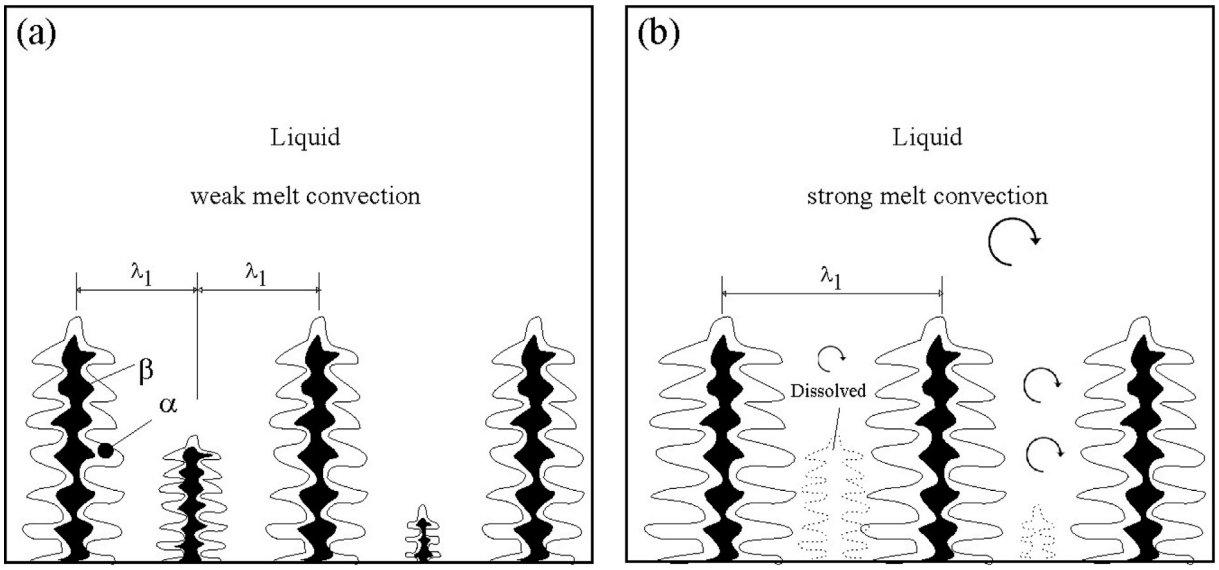

Fig. 6. Schematic diagram comparing the growth of primary dendrites under (a) weak and (b) strong melt convection conditions.

in Fig. 7.

Because the relatively high cooling rates used in industrial processing, the completion of the peritectic reaction is rarely observed. This is because β surrounds α and the peritectic reaction is stifled since L cannot reach α [29]. The isolation of the liquid also depends on the morphologies of the phases growing in concurrence in a certain peritectic alloy. The Sn-2 wt.%Sb alloy is a monophasic composition, and possibly, tends to form the β-Sn phase before the peritectic reaction is attained. Due to the non-equilibrium solidification, local accumulation of Sb ahead the solidification interface is induced, which contributes to the peritectic reaction to take place. It appears that the cellular morphology obtained for higher cooling rates favor the liquid to reach the α phase in order to produce β. As a result, finer α layers related to the incomplete reaction will be formed as seen in Fig. 8(a and b). Oppositely, the more intricate dendritic morphology tends to isolate the α phase from the liquid, and as a result, the formation of β from the peritectic reaction can no longer take place. Thicker α layers characterize the resulting microstructure as observed in Fig. 8(c and d).

Fig. 9 (a) shows examples of the engineering stress vs. engineering strain curves obtained for samples associated with different cooling rates and microstructures. Magnified views of the data in Fig. 9(a) are shown as Fig. 9(b)–(d) for the cooling rates 0.9 K/s, 0.1 K/s and 0.03 K/s respectively. A homogeneous deformation stage preceded the start of the PLC effect in the samples of the investigated alloy. With basis on counting the formed serrations in all generated plots, it is conceived that the first average PLC band was at 24% ± 3% strain. The bands emerge roughly for the same level of deformation in all tests.

The serration average amplitude increases with increasing the cellular/dendritic spacing (λ_1), with the experimentally mean amplitudes being 1.2 ± 0.3 MPa, 3.8 ± 0.5 MPa, 4.1 ± 0.1 MPa and 4.3 ± MPa for the samples having $\lambda_c = 99\,\mu m$ (β-Sn cells), $\lambda_1 = 179\,\mu m$ (β-Sn dendrites), $\lambda_1 = 225\,\mu m$ and $\lambda_c = 261\,\mu m$ respectively. High cellular/dendritic spacing generates a higher PLC band amplitude as compared to low spacing. Furthermore, the serration type switches from type A in the samples associated with cellular microstructrure to type B in the dendritic microstructure samples.

It seems reasonable to assume that the stress-induced diffusion is more efficient in the case of the samples having fine cellular spacing. Thus, the solute is more available to repeatedly block and release the mobile dislocations during the plastic regime. As a result, smaller and more spaced PLC bands prevailed in the cellular arranged samples, as observed in Fig. 9(b).

The results of the tensile tests are summarized in Fig. 10, where the ultimate tensile strength (σ_u), and elongation (δ) are related either to the cellular spacing or to the primary dendrite arm spacing.

It can be realized that the changes in the dendritic spacing do not affect the alloy strength, while such changes may have a considerable impact on ductility.

The best microstructural arrangement combining both strength and ductility for the Sn-2 wt.%Sb alloy is the cellular one, that is a strength of 27 MPa and a ductility of 51%. This can be probably explained by the prevalence of very fine Sn-rich cells reinforced by finer scaling SnSb layers as found for positions nearer the bottom of the alloy casting.

4. Conclusions

Sn-2 wt.%Sb alloy castings were directionally solidified with a 100 μm-thick ceramic layer on the cooled surface of the bottom part of the mold with a view to decreasing the cooling rates during solidification. The evolution of microstructural morphologies; length scale of the β-Sn matrix and tensile properties along the length of the castings were investigated and the following

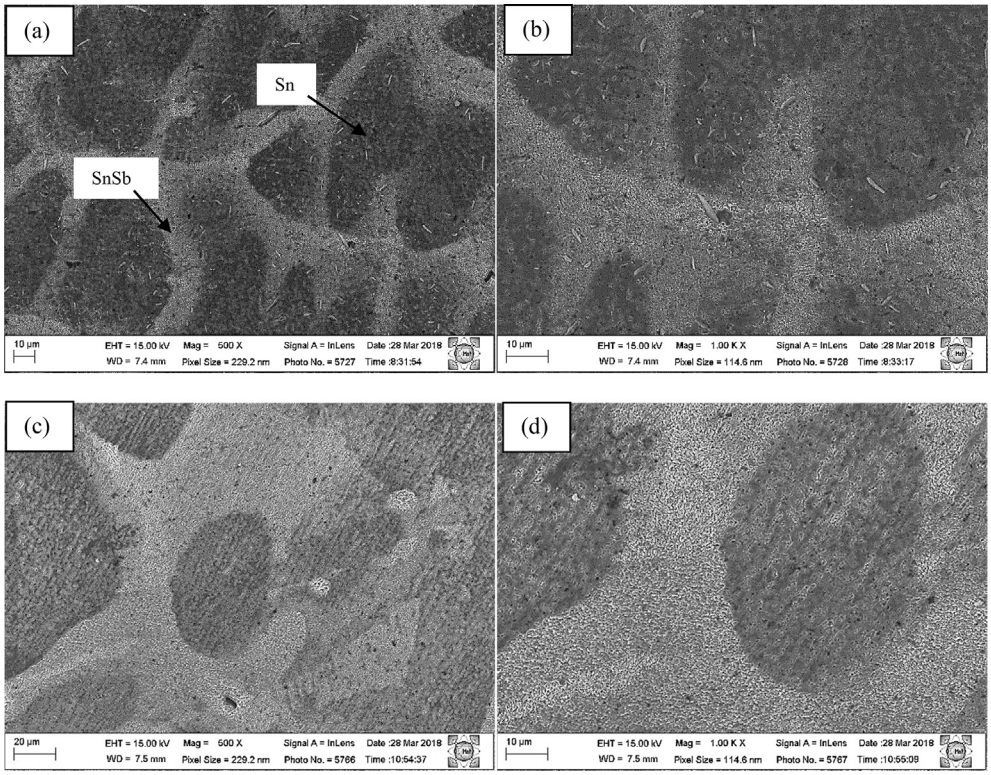

Fig. 8. SEM images highlighting the sizes of both β-Sn and SnSb phases throughout the Sn-2 wt.%Sb alloy microstructures: (a,b) cells, $\dot{T} = 1.1$ K/s; and (c,d) dendrites, $\dot{T} = 0.07$ K/s.

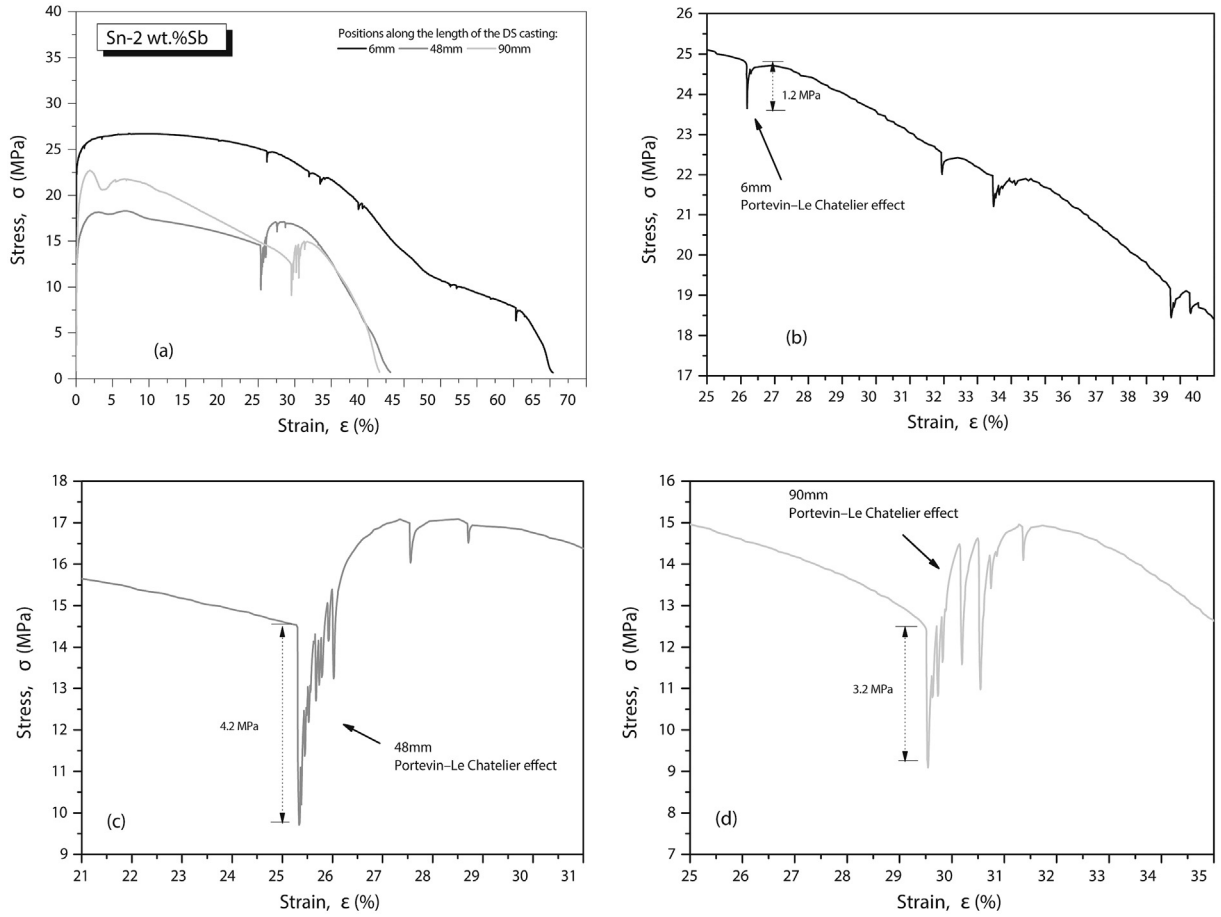

Fig. 9. (a) Typical stress x strain diagrams for the Sn-2 wt.%Sb samples solidified at three distinct solidification cooling rates; and (b,c,d) details of onsets, magnitudes and shapes of the serrations in the stress-strain curves.

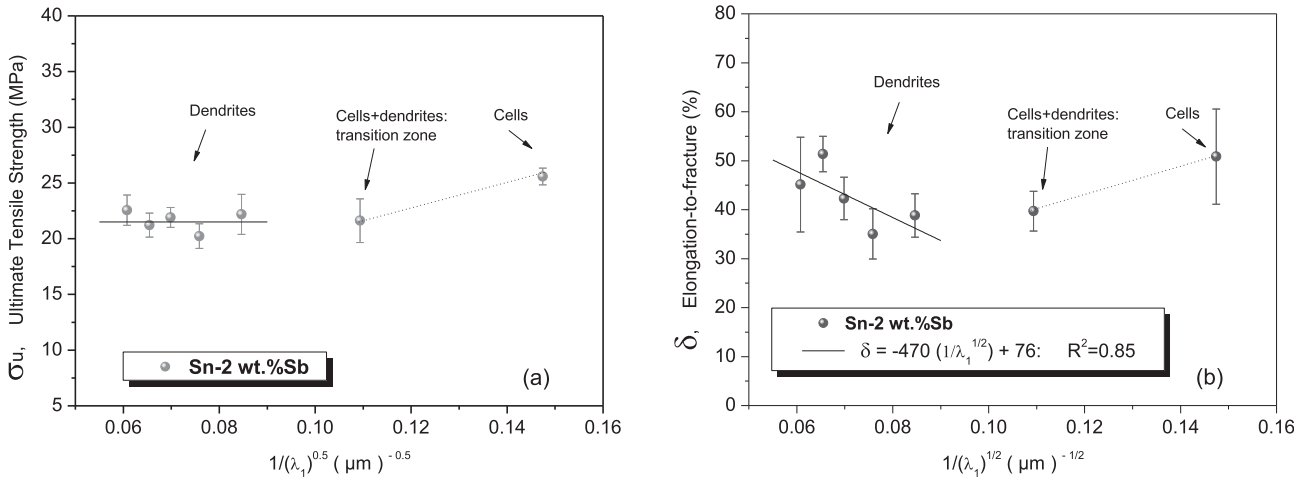

Fig. 10. (a) Ultimate tensile stress; and (b) elongation, as a function of the cellular/primary dendritic spacing for the Sn-2 wt%Sb solder alloy.

conclusions can be drawn:

The β-Sn matrix was shown to have a cellular morphology for cooling rates (Ṫ) higher than 1 K/s and after experiencing a reverse cellular/dendritic transition, a dendritic pattern prevailed for Ṫ<0.3 K/s. The alloy microstructure is constituted by this β-Sn matrix surrounded by the Sn-Sb (α) phase.

The following experimental power functions relating the primary dendritic arm spacing (λ_1: μm) to the cooling rate, $\lambda_1 = 70\ (\dot{T})^{-0.5}$ and $\lambda_1 = 118\ (\dot{T})^{-0.55}$, were shown to represent the dendritic growth for castings solidified under weak and strong conditions of melt convection, respectively.

The tensile tests were shown to be characterized by the occurrence of the Portevin – Le Chatelier (PLC) effect, in which a homogeneous deformation stage preceded the start of serrations of

stresses. The serration average amplitude increased with increasing cellular/dendritic spacings and was found to be lower in the specimens of cellular microstructures as compared to those of dendritic morphology.

The best microstructural arrangement combining both tensile strength and ductility was shown to be the cellular one, that is an ultimate strength of 27 MPa and a ductility of 51%, which seems to be caused by the prevalence of very fine Sn-rich cells reinforced by fine scaling SnSb layers.

Acknowledgements

The authors are grateful to FAPESP- São Paulo Research Foundation, Brazil (grant 2017/12741-6), Capes- Coordenação de Aperfeiçoamento de Pessoal de Nível Superior, Brazil (Funding Code 001); and CNPq- National Council for Scientific and Technological Development, Brazil (grants 400506/2016-5 and 301600/2015-5).

References

[1] European Parliament, Directive 2011/65/EU on the restriction of the use of certain hazardous substances in electrical and electronic equipment, Off. J. Eur. Union 54 (2011) 88–110.
[2] R.A. Islam, Y.C. Chan, W. Jillek, S. Islam, Comparative study of wetting behavior and mechanical properties (microhardness) of Sn–Zn and Sn–Pb solders, Microelectron. J. 37 (2006) 705–713.
[3] J. Koo, C. Lee, S.J. Hong, K.-S. Kim, H.M. Lee, Microstructural discovery of Al addition on Sn–0.5 Cu-based Pb-free solder design, J. Alloy. Comp. 650 (2015) 106–115.
[4] H. Kerr, W. Kurz, Solidification of peritectic alloys, Int. Mater. Rev. 41 (1996) 129–164.
[5] T. Umeda, T. Okane, W. Kurz, Phase selection during solidification of peritectic alloys, Acta Mater. 44 (1996) 4209–4216.
[6] W. Zhai, B. Wei, Peritectic solidification characteristics of Sb–Sn alloy under ultrasonic vibration, Mater. Lett. 138 (2015) 1–4.
[7] S. Smith, G. Zeng, J. Read, S.D. McDonald, K. Nogita, Peritectic reactions and phase transformations of Sn-30wt%Cu for high temperature Pb-Free soldering applications, Mater. Sci. Forum 857 (2016) 58–62.
[8] M. Dias, T. Costa, O. Rocha, J.E. Spinelli, N. Cheung, A. Garcia, Interconnection of thermal parameters, microstructure and mechanical properties in directionally solidified Sn–Sb lead-free solder alloys, Mater. Char. 106 (2015) 52–61.
[9] A.A. El-Daly, A. Fawzy, A.Z. Mohamad, A.M. El-Taher, Microstructural evolution and tensile properties of Sn–5Sb solder alloy, containing small amount of Ag and Cu, J. Alloy. Comp. 509 (2011) 4574–4582.
[10] G. Zeng, S. McDonald, K. Nogita, Development of high-temperature solders: review, Microelectron. Reliab. 52 (2012) 1306–1322.
[11] R.W. Messler, Joining of Materials and Structures: from Pragmatic Process to Enabling Technology, Butterworth-Heinemann, Oxford, 2004.
[12] M.M. El-Bahay, M.E. El Mossalamy, M. Mahdy, A.A. Bahgat, Study of the mechanical and thermal properties of Sn–5 wt.%Sb solder alloy at to annealing temperatures, Phys. Status Solidi A 198 (2003) 76–90.
[13] R.K. Mahidhara, S.M.L. Sastry, I. Turlik, K.L. Murty, Deformation and fracture behavior of Sn–5%Sb solder, Scr. Metall. Mater. 31 (1994) 1145–1150.
[14] M.J. Esfandyarpour, R. Mahmudi, Microstructure and tensile behavior of Sn–5Sb lead-free solder alloy containing Bi and Cu, Mater. Sci. Eng. A Struct. 530 (2011) 402–410.
[15] S.W. Chen, C.C. Chen, W. Gierlotka, A.R. Zi, P.Y. Chen, H.J. Wu, Phase equilibria of the Sn–Sb binary system, J. Electron. Mater. 37 (2008) 992–1002.
[16] J.H. Kim, S.W. Jeong, H.M. Lee, Thermodynamics-aided alloy design and evaluation of Pb free solders for high-temperature applications, Mater. Trans. 43 (2002) 1873–1878.
[17] O.L. Rocha, T.A. Costa, M. Dias, A. Garcia, Cellular/dendritic transition, dendritic growth and microhardness in directionally solidified monophasic Sn–2%Sb alloy, Trans. Nonferrous Metals Soc. China 28 (2018) 1679–1686.
[18] A. Yilmaz, The Portevin–Le Chatelier effect: a review of experimental findings, Sci. Technol. Adv. Mater. 12 (2011) 063001 1–06300116.
[19] J.E. King, C.P. You, J.F. Knott, Serrated yielding and the localized shear failure mode in aluminium alloys, Acta Metall. 29 (1981) 1553–1566.
[20] G. Ananthakrishna, Current theoretical approaches to collective behavior of dislocations, Phys. Rep. 440 (2007) 113–259.
[21] Y. Cai, S. Yang, S. Fu, D. Zhang, Q. Zhang, Investigation of Portevin–Le Chatelier band strain and elastic shrinkage in Al-based alloys associated with Mg contents, J. Mater. Sci. Technol. 33 (2017) 580–586.
[22] J.E. Spinelli, N. Cheung, A. Garcia, On array models theoretical predictions versus measurements for the growth of cells and dendrites in the transient solidification of binary alloys, Phil. Mag 91 (2011) 1705.
[23] D.M. Rosa, J.E. Spinelli, I.L. Ferreira, A. Garcia, Cellular growth during transient directional solidification of Pb–Sb alloys, J. Alloys Compd 422 (2006) 227.
[24] D.M. Rosa, J.E. Spinelli, A. Garcia, Tertiary dendrite arm spacing during downward transient solidification of Al–Cu and Al–Si alloys, Mater. Let 60 (2006) 1871.
[25] C.B. Cruz, R. Kakitani, B.L. Silva, M.G.C. Xavier, A. Garcia, N. Cheung, J.E. Spinelli, Transient unidirectional solidification, microstructure and intermetallics in Sn-Ni alloys, Mater. Res. 21 (2018), e20171099.
[26] M.G.C. Xavier, C.B. Cruz, R. Kakitani, B.L. Silva, A. Garcia, N. Cheung, J.E. Spinelli, Directional solidification of a Sn-0.2Ni solder alloy in water-cooled copper and steel molds: related effects on the matrix micromorphology, nature of intermetallics and tensile properties, J. Alloy. Comp. 723 (2017) 1039–1052.
[27] T. Takemoto, M. Takemoto, Dissolution of stainless steels in molten lead-free solders, Solder. Surf. Mt. Technol. 18 (2006) 24–30.
[28] X. Hu, S. Li, S. Gao, L. Liu, H. Fu, Effect of melt convection on primary dendrite arm spacing in directionally solidified Pb-26%Bi hypo-peritectic alloys, Trans. Nonferrous Metals Soc. China 21 (2011) 65–71.
[29] F.C. Campbell, Phase Diagrams – Understanding the Basics, ASM International, Ohio, 2012.